PHILOSOPHICAL TRANSACTIONS OF THE ROYAL SOCIETY A MATHEMATICAL, PHYSICAL & ENGINEERING SCIENCES

Deformed Rocks and their Textures [and Discussion]

A. W. B. Siddans and N. J. Soper

Phil. Trans. R. Soc. Lond. A 1976 **283**, 43-54
doi: 10.1098/rsta.1976.0068

Phil. Trans. R. Soc. Lond. A. **283**, 43–54 (1976) [43]
Printed in Great Britain

Deformed rocks and their textures

By A. W. B. Siddans
Earth Sciences Department, University of Leeds

Modern analytic methods enable finite strain states on the scale of a hand specimen and textures on a much smaller scale to be determined in some rocks, together with error measures. Some recent publications describe attempts to calculate finite strain states from observed textures of phyllosilicates in slates. Petrographic, finite strain and textural data for several slates are presented, which suggest that such calculations are in fact often impossible and in general give inconsistent and erroneous results. The reasons for this are discussed, and it is suggested that there are no simple relations between finite strain states and textures in slates.

Introduction

Some recent publications (Oertel 1970, 1974) describe attempts to relate phyllosilicate textures to finite strain states in slates, according to the model of deformation proposed by March (1932). In order to assess the validity of this assumed relation finite strain states and phyllosilicate textures have been determined in three groups of slates:

(i) 'Bird's-eye tuffs' from the Borrowdale Volcanic Group, of Ordovician age, from the English Lake District.

(ii) 'Bird's-eye tuffs' from the Capel Curig Volcanic Group, of Ordovician age, from North Wales.

(iii) The 'terres noires' of Jurassic age, from the External Zone of the French Alps.

Since assessment of the March model relation depends upon comparing numeric parameters of finite strain and texture, it is essential to consider how the necessary finite strain and texture analyses are made, and what errors may arise in their quantification.

Finite strain analysis

In the case of the 'terres noires' samples, strain states were computed from the shapes of ammonites, by using the method of Tan (1973) and Ramsay (1967, pp. 148–149). The only check on the validity of strain analyses made by such methods is to repeat the analysis several times for several fossils at the same location.

In the case of the 'bird's-eye tuffs' finite strain analysis involves three stages of measurement and computation:

(i) Measurement of individual ellipses resulting on section planes through aggregates of ellipsoidal markers.

(ii) Computation of the strain ellipse in each of three mutually perpendicular section planes.

(iii) Combination of the strain ellipses to give the finite strain ellipsoid.

If the measured shapes are not perfectly elliptical, inaccuracies may be introduced into the analysis at the first stage, be compounded during the second, and result in internally inconsistent

two-dimensional data. It is thus necessary to have some test for ellipticity incorporated into the measurement stage.

Measurement of individual ellipses

The equation of an ellipse with semi-axes $\lambda_1^{\frac{1}{2}}$ and $\lambda_2^{\frac{1}{2}}$ ($\lambda_1 > \lambda_2$), with its centre at the origin and long axis at θ to the x-axis, is of the form:

$$\lambda'_x\, x^2 - 2\gamma'_{xy}\, xy + \lambda'_y\, y^2 = 1. \tag{1}$$

Its semi-axes and long axis orientation may be calculated from the invariants (Ramsay 1967, pp. 82–83), once the values of λ'_x, λ'_y and γ'_{xy} are known.

In our laboratory at Leeds we now analyse elliptical shapes on photographs of sections cut through aggregates of ellipsoidal markers, by use of a *D*-mac digitizer on-line with a Digico Micro 16V minicomputer. A reference direction *Ox* is defined, usually parallel to a bedding or cleavage trace, then for each ellipse the following procedure is followed:

(i) Trace round the ellipse with the *D*-mac follower, automatically collecting a minimum of 20 pairs of coordinates from the periphery of the ellipse.

(ii) Compute the geometric centre of the ellipse and transpose all coordinates to refer to that as origin.

(iii) Compute the area of the ellipse and scale the coordinates to make the area π.

(iv) Select 20 equidistantly spaced pairs of coordinates and set up 20 linear equations of the form (1).

(v) Solve the overdetermined linear equation system for λ'_x, λ'_y and γ'_{xy}, and hence compute the axial ratio and long axis orientation.

(vi) Compute an error measure for non-ellipticity by substituting the 20 pairs of coordinates into:

$$\text{error} = \sum_{m=1}^{20} (x_m^2\, \lambda'_x - 2x_m\, y_m\, \gamma'_{xy} + y_m^2\, \lambda'_y - 1). \tag{2}$$

In practice it is found that the error measure increases rapidly with small departures from ellipticity, so that some pre-set value can be assigned to eliminate data with a higher error from subsequent computations.

Computation of the strain ellipse in a section plane

Techniques for computation of the strain ellipse in a section plane through an aggregate of ellipsoidal shapes that have deformed homogeneously with their matrix, have been given by Dunnet (1969), Elliott (1970) and Dunnet & Siddans (1971).

Combination of two-dimensional strain data

As noted by Helm & Siddans (1971) and Roberts & Siddans (1971), there are six independent ways of combining two-dimensional strain data on three mutually perpendicular section planes, to give the finite strain ellipsoid. Mutual inconsistencies within the two-dimensional data give rise to a spread of results in both axial ratios and orientations for the ellipsoid, which may be illustrated conveniently on a Flinn diagram and stereoplot of axial orientation (see, for example, Helm & Siddans 1971, figures 2*d*, 3).

The scale of finite strain analyses

The volume of rock involved in such finite strain analyses depends upon the size of the strain markers used. For oolites it is usually of the order of tens of cubic centimetres, while for 'bird's-

eye tuffs' it may be two orders of magnitude greater. Such strain analyses are thus on a scale suitable for the restoration of fossils or sedimentation structures to their pre-deformation state, but as Ramsay (1967, p. 54) notes, probably do not apply to deformation on the scale of individual grains. Indeed, Whalley (1973) described mutually inconsistent two-dimensional strain data based on deformation of detrital quartz grains in Ordovician slates from Rhosneigr, North Wales, and Knipe (1974) demonstrated that the deformation of such quartz grains differs from the amount of deformation recorded by green spots in purple Cambrian slates from Penrhyn, North Wales, and by the lapilli in the 'bird's-eye tuffs' from Capel Curig discussed in this study.

Texture goniometry

The texture goniometer is an attachment to a diffractometer that enables a specimen to be rotated into all orientations once the diffractometer has been set to a specific Bragg angle. It can be used in either reflexion or transmission modes.

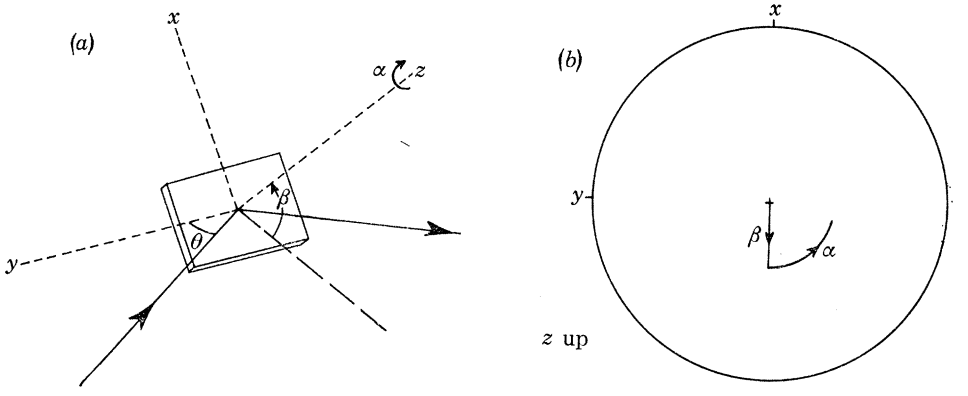

Figure 1. (*a*) The geometry of reflexion mode texture goniometry. (*b*) Stereoplot of positions of poles to lattice planes satisfying the Bragg law, when the specimen is tilted through an angle β, then rotated through an angle α in its own plane.

Reflexion mode

Reflexion mode operation of the texture goniometer was first described by Schulz (1949). The geometry of this mode and rotation nomenclature are shown in figure 1. A thick slice is used with one flat surface situated at the goniometer centre, normal to the bisector of the angle between the incident X-ray beam and the detector arm. Rotation β tilts the specimen out of this 'normal' position, and rotation α rotates the specimen in its own plane. If the rate of rotation β is very slow relative to α, normals to lattice planes satisfying the Bragg law trace out a spiral on a stereoplot referred to known specimen coordinates. Alternatively, a step-scanning procedure may be followed, as in our laboratory at Leeds, so that intensity data is collected at specific points around small circles. Advantages of reflexion mode operation are:

(i) Ease of specimen preparation.

(ii) The effective volume of scattering material is constant for all values of tilt β, providing the surface area of the specimen is large enough.

Disadvantages of reflexion mode operation are:

(i) As the specimen is tilted part of it moves inside the focusing circle of the diffractometer, part of it moves outside. This leads to the diffracted beam coming to a focus over a range of

angles 2θ, so that the diffraction peak is broadened. As the detector slits view a small range of angles 2θ, a loss of recorded intensity results. This is the phenomenon of 'geometric defocusing', and the intensity loss resulting from it must be corrected for. Various correction procedures have been suggested (Feng 1965; Baker *et al.* 1969; Tenckhoff 1970; Couterne & Cizeron 1971). Of these the empirical corrections of Baker *et al.* and Tenckhoff are not in general possible, as they depend on having available samples of identical material with no preferred orientation. My own experiments with such materials as are available, have shown that Feng's analytic correction is quite adequate.

(ii) As the specimen is tilted the depth of penetration of the incident X-rays decreases, while the surface area irradiated by the incident beam increases. At high tilts some of the beam misses the specimen. For this reason reflexion mode scans are terminated at tilts of 60–70°, depending on specimen size, beam size and Bragg angle.

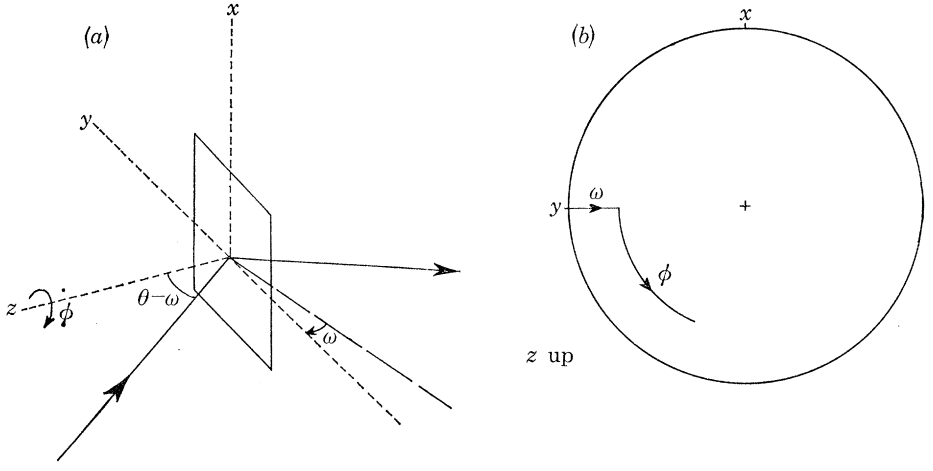

FIGURE 2. (*a*) The geometry of transmission mode texture goniometry. (*b*) Stereoplot of positions of poles to lattice planes satisfying the Bragg law, when the specimen is tilted through an angle ω, then rotated through an angle ϕ in its own plane.

Transmission mode

Transmission mode operation of the texture goniometer was first described by Decker *et al.* (1948). The geometry of this mode and rotation nomenclature are shown in figure 2. A thin slice with parallel flat sides is used, with its centre situated at the goniometer centre, vertical in the plane of the bisector of the angle between the incident X-ray beam and the detector arm. Rotation ω tilts the specimen out of this plane, about a vertical axis (cf. rotation θ), and rotation ϕ rotates the specimen in its own plane (cf. rotation β in reflexion mode). If the specimen is tilted through a small angle ω, then rotated through 360° in its own plane, normals to lattice planes satisfying the Bragg law trace out a small circle on a stereoplot referred to known specimen coordinates. The main advantage of transmission mode operation is the greater penetration of the X-ray beam. Disadvantages are:

(i) More difficult specimen preparation and handling.

(ii) There is a change in effective volume of scattering material with increase in tilt ω, leading to an intensity loss. This can be corrected for analytically (Bragg & Packer 1964, equation 9). The absorption term μt in this equation is easily measured for the specimen by recording the

intensity of a standard diffraction peak with and without the specimen placed over the detector slits, and substitution into the equation:

$$I/I_0 = e^{-\mu t}. \quad (3)$$

The background intensity is also subject to this intensity loss. At high tilts the specimen mount starts to shadow the specimen, so that transmission mode scans are terminated at 20–30°, according to the corresponding range of reflexion mode data.

Combination of data for a complete pole figure

Because of the limitations on tilt in both reflexion and transmission modes, sufficient data to cover the whole pole figure cannot be obtained from a single scan in either mode. It is thus necessary to combine data from either (figure 3):

(i) 1 reflexion + 1 transmission scan on same section plane.
(ii) 3 reflexion scans on 3 mutually perpendicular section planes.
(iii) 3 transmission scans on 3 mutually perpendicular section planes.

We prefer the first of these procedures, in which the specimen is removed from the goniometer at the end of all the reflexion mode work, and ground to a thin slice. Transmission scans can then begin on the same small circle that terminated the reflexion mode scans, making scaling of the data a simple analytic procedure. This method also has the advantage that in part at least, the reflexion and transmission mode work is done on the same part of the specimen. Either of the other two methods necessitates that three different parts of the specimen be used, i.e. faces of a cube. Scaling of the three sets of data is also more complex, involving matching of contours on the corrected data, while any errors in the correction procedures will tend to give the resulting pole figure a spurious orthorhombic symmetry.

Normalization of the intensity data

The intensity data, after correction for defocusing and/or absorption, subtraction of background and scaling, has to be normalized, so that the pole figure can be presented in terms of multiples of random texture intensity, rather than count rates unique to that specimen and experiment. This is easily done when the combined reflexion/transmission mode procedure is used on a step-scanning instrument, with equal angular increments both between and around small circles, when the direct analytic method of Bragg & Packer (1964, equation 14) can be programmed. In other cases the more complex process of contouring the combined and corrected intensity data at arbitrary count rates, making planimetric estimates of the areas between successive contours, and estimation of the mean intensity for each fractional area, then recalibrating the contours, as described by Oertel (1970), must be used.

Counting errors

All intensity measurements have statistical errors associated with them, which may be conveniently expressed as a probable fractional error, ϵ_{50} (see, for example, Parrish 1962). Such errors are associated not only with measurements of the raw intensity data on the diffraction peak, but also with the background and absorption term measurements. In all the necessary computations to produce a pole figure these errors are cumulative. If continuous-scanning, or step-scanning with a constant counting time at each data point techniques are used, these errors are maximized when the count rate is at a minimum. Obviously the step-scanning method,

PHILOSOPHICAL TRANSACTIONS OF THE ROYAL SOCIETY A MATHEMATICAL, PHYSICAL & ENGINEERING SCIENCES

when used to measure time required to accumulate a pre-set number of counts, would enable these errors to be made more uniform.

Description and symmetry of pole figures

It is difficult not to be cynical about the symmetry that some published pole figures are claimed to have, especially when no statement about how the pole figure was produced, or to what extent the data was smoothed, is given. A simple method of assessing pole figure symmetry for planar and/or linear textures is by a method of moments technique, in which the normalized intensity data is entered into small sampling circles equidistantly spaced on the projection hemisphere. The covariance matrix of direction cosines, referred to known specimen coordinates, is set up and diagonalized to give the principal axes of the distribution of pole densities

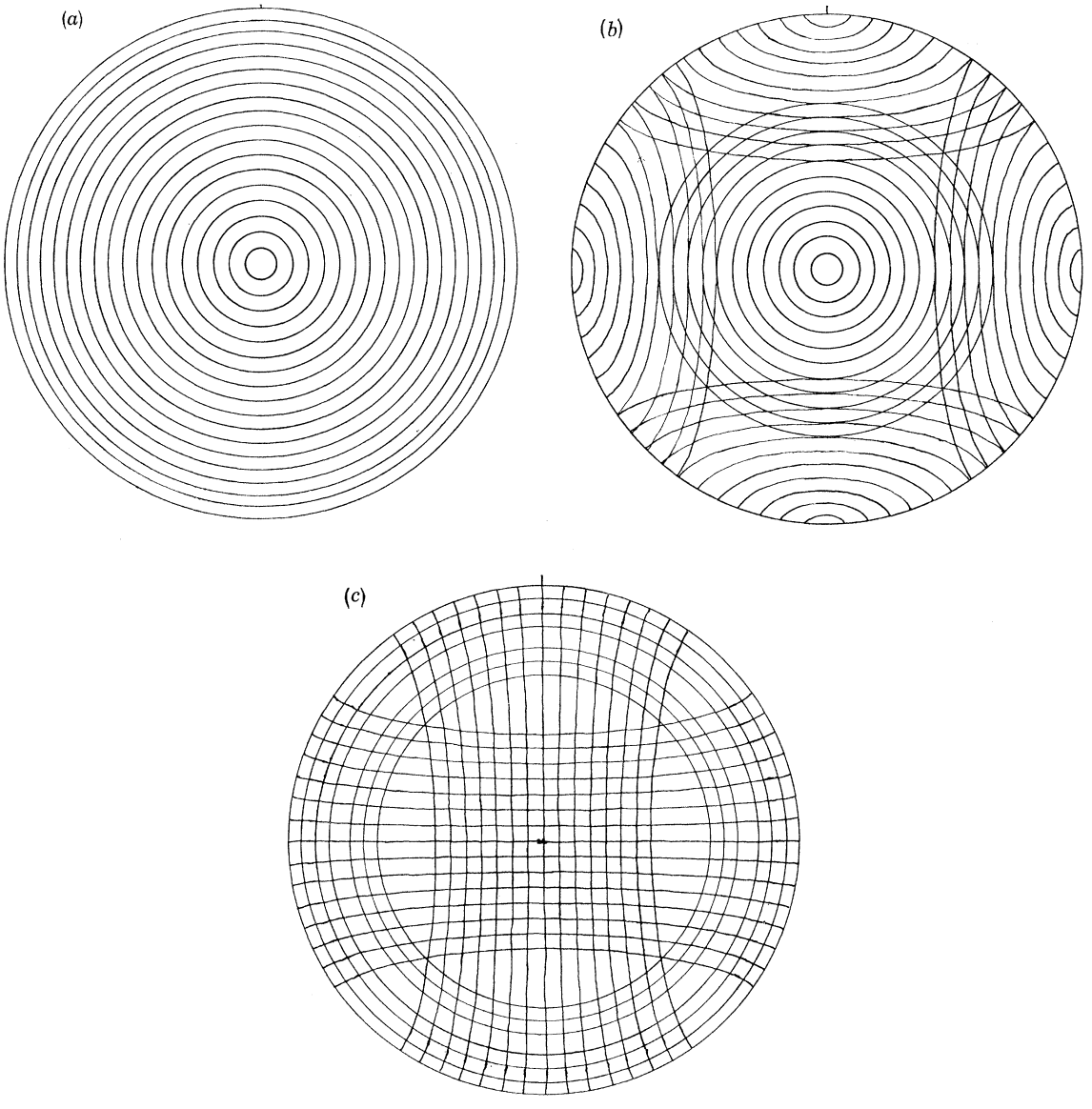

FIGURE 3. Combination of data from individual scans to complete the pole figure. (*a*) Reflexion + transmission scans. (*b*) Three reflexion scans. (*c*) Three transmission scans. Small circles are shown 5° apart.

PHILOSOPHICAL TRANSACTIONS OF THE ROYAL SOCIETY A MATHEMATICAL, PHYSICAL & ENGINEERING SCIENCES

best fitting to an orthorhombic model. The second moments and skewness of the distribution about the principal axes can then be computed. The second moments measure the dispersion of lattice planes about the principal axes, ranging from 0 for perfect parallelism, to 1 when all planes are normal to an axis. Skewness measures the degree of asymmetry of the distribution about an axis, being 0 when symmetry is perfect. Low skewness about two axes implies high symmetry about the plane defined by those axes. Thus a random texture has all three second moments the same, and an axially symmetric texture has two second moments the same with low skewness about the third.

A more rigorous description of a pole figure, not limited to planar or linear textures, is given by expanding the intensity data as a series of spherical harmonics (Roe 1965). In the assessment of pole-figure symmetry maximum benefit is obtained when the specimen cordinates are arranged parallel to as many symmetry axes as possible, then mirror planes of symmetry are readily assessed.

Some results

Pole figures for chlorite and muscovite (illite) basal planes have been measured for samples of known finite strain states, from three groups of slates, and the results compared with the textures predicted by the March model as far as was possible. Assuming an initial random texture, the variation in pole density with shortening or stretching in any direction, as predicted

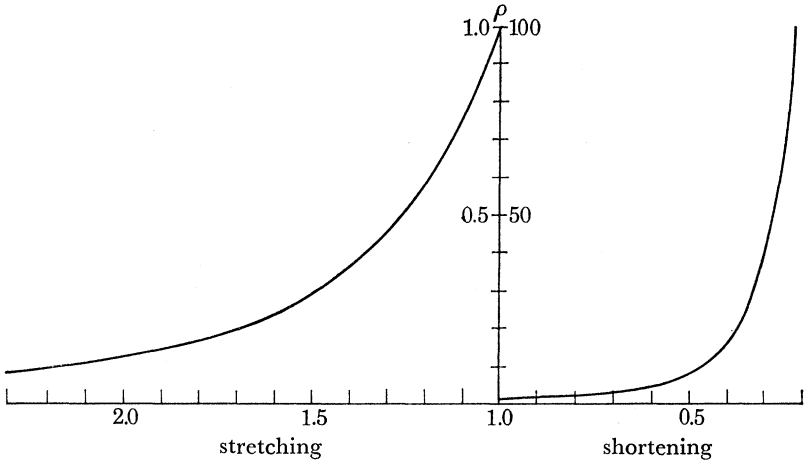

FIGURE 4. The relation between pole density in any direction and the amount of stretching or shortening in that direction, according to the March model.

by the March model, is illustrated in figure 4. It is apparent from this diagram that in the field of finite stretching it is necessary to be able to define the pole density to at least two decimal places. In practice this is found to be impossible. For example in the pole figure shown in figure 5, the pole density along the maximum finite extension drection, X, is indistinguishable from 0.00, and has a probable fractional error of 33 %. Further difficulty in making comparisons with the March model predictions arose because none of the pole figures had the required orthorhombic symmetry, they were all triclinic in detail. Thus it was only found possible to compare observed pole densities along the maximum finite shortening axis with the March model predictions. This is done for the three groups of slates in figures 6, 7 and 8. The samples were chosen for texture analysis within each group, with low error measures associated with their finite strain determinations. Since the maximum pole density is found parallel to the direction

PHILOSOPHICAL TRANSACTIONS OF THE ROYAL SOCIETY A MATHEMATICAL, PHYSICAL & ENGINEERING SCIENCES

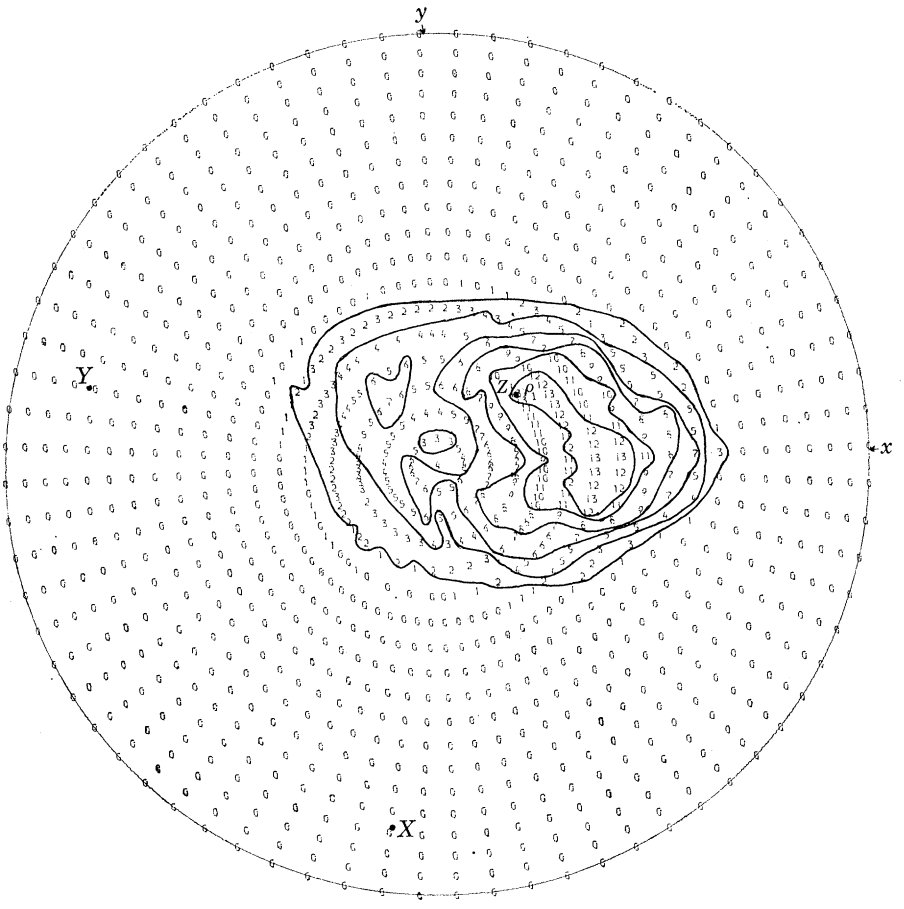

FIGURE 5. Pole figure for muscovite basal planes in a 'bird's-eye tuff' from Capel Curig, North Wales. Plot is equal area upper hemisphere (z up) referred to specimen coordinates. Contours at 2, 4, 6, 8, 10 and 12 × random; $\rho_1 = 13.8$; $\epsilon_{50} = 0.018$; $X:Y:Z = 1.54:1.14:0.57$; $\rho_1^* = 5.5$ (March model prediction).

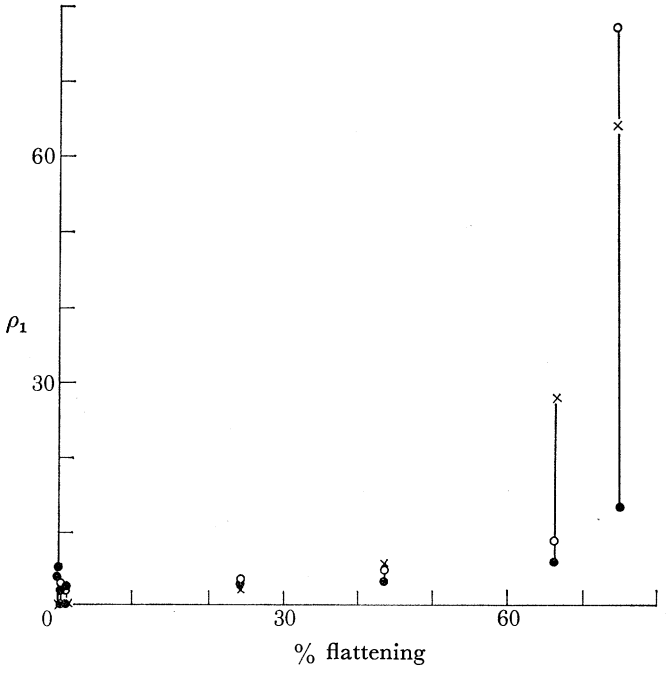

FIGURE 6. Variation in maximum pole densities for chlorite basal planes (●) and muscovite basal planes (○) with percentage flattening, in a group of slaty rocks from the 'terres noires', French Alps. The March model predictions are shown as crosses.

of maximum finite shortening, it follows that minimum probable fractional errors are associated with these pole densities.

It is clear from the results shown in figures 6, 7 and 8 that not only do the maximum pole densities differ from those predicted by the March model, but that within a single specimen chlorite and muscovite may have different textures. Similar results have been found in Ordovician slates from Rhosneigr, North Wales (Whalley, 1973), and in deformed Torridonian rocks from Scotland (Coward & Whalley, personal communication).

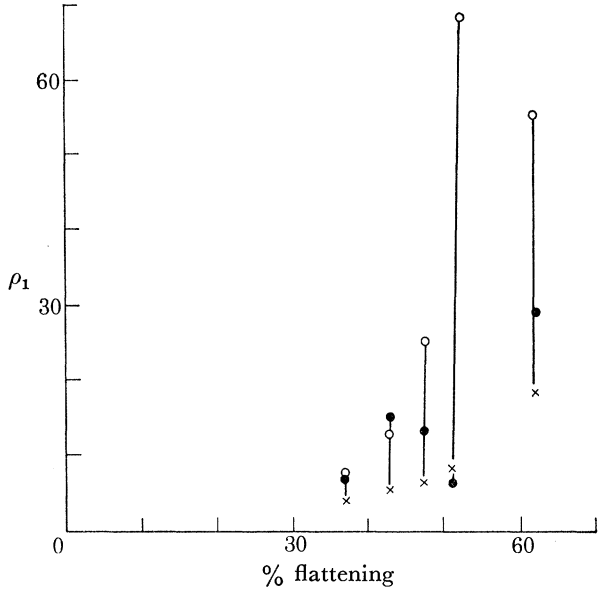

FIGURE 7. Variation in maximum pole densities for chlorite basal planes (●) and muscovite basal planes (○) with percentage flattening, in a group of slaty 'bird's-eye tuffs' from Capel Curig, North Wales. The March model predictions are shown as crosses.

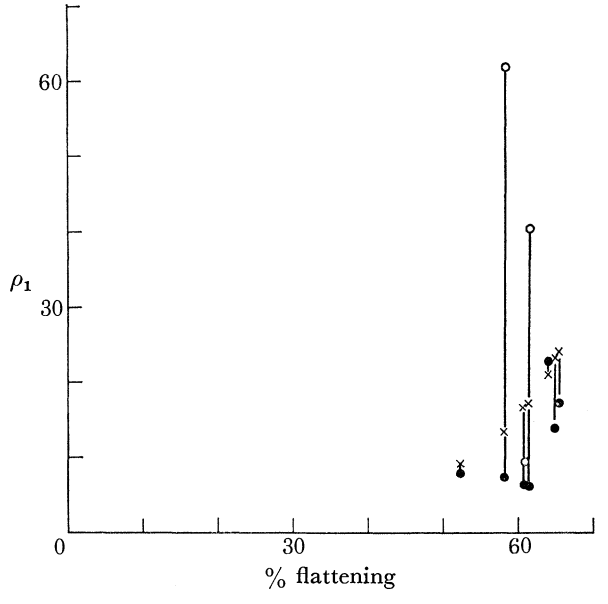

FIGURE 8. Variation in maximum pole densities for chlorite basal planes (●) and muscovite basal planes (○) with percentage flattening, in a group of slaty 'bird's-eye tuff's' from the English Lake District. The March model predictions are shown as crosses.

PHILOSOPHICAL TRANSACTIONS OF THE ROYAL SOCIETY A MATHEMATICAL, PHYSICAL & ENGINEERING SCIENCES

Discussion

As used by Oertel (1970, 1974) the March model assumes a starting material that is a randomly oriented aggregate of platy clay minerals, that deform homogeneously with the rock as a whole, all diagenetic/metamorphic reactions producing new minerals by growth on nuclei whose orientation is controlled by the pre-existing texture. Thus the end product of compaction and tectonic deformation is always an orthorhombic texture, whose principal axes are quantitively related to the principal axes of the total deformation ellipsoid.

Without doubt burial and compaction does often lead to the development of a bedding plane texture in clay minerals. But it appears that in some cases clay minerals may be deposited in a highly oriented way, and that the relation between amount of compression and degree of preferred orientation is not a simple one (see recent discussion by Moon (1972)). For example, a standard way of producing highly oriented clay samples in the laboratory is to sediment them fast onto a porous tile; and beds within the Nant Pig Mudstones (Cambrian of North Wales) still exist as mudstones sandwiched between shales.

Diagenetic/metamorphic reactions may often produce new minerals by growth on pre-existing nuclei, hence with the same texture as the pre-existing phyllosilicates. However this is not always the case. Breakdown of mixed layer illite-montmorillonite with increase in temperature, produced new phyllosilicates that grew perpendicular to clastic quartz grains in the Quartenschiefer of the Glarus Alps (Frey 1970). Etheridge & Lee (1975) describe bimodal mica orientations in slates from Lady Loretta, Queensland, where it appears that large micas of diagenetic origin remain parallel to bedding, while new micas that grew during deformation have grown parallel to cleavage. Oertel (1970) has suggested that the high degree of preferred orientation of phyllosilicates in 'bird's-eye tuffs' of the Borrowdale Volcanic Group is due to post-tectonic recrystallization.

Clearly phyllosilicates do not behave as purely passive markers during deformation. If they were free to contract or extend according to orientation in the finite strain ellipsoid, these deformations would result in changes in lattice spacings, and hence shifts in diffraction peaks, and texture goniometry would be impossible. In fact recent electron microscopy on the Ordovician slates of Rhosneigr (White 1974, fig. 2) has shown that micas become bent, impinge upon each other and upon other mineral species, for example quartz grains. Indeed, Oertel & Phakey (1972) note that phyllosilicates must have been able to dissolve at contact points with interstitial quartz, then reappear between these points.

Experimental evidence suggests that aggregates of platy grains do not deform according to the March model. Clark (1970) found that the March model did not explain the observed textures seen in his experimentally deformed dense kaolinite-water systems. Means & Paterson (1966) concluded that similarities between observed textures in their experiments, and March model predictions from the known strains, were fortuitous.

There is no logical reason why textures in slates should be quantitively related to finite strain states. With the exception of mimetic recrystallization, the texture producing processes that effect phyllosilicates are, as noted by Etheridge & Lee (1975), controlled by local stresses operating on the scale of strain increments, which need not be superposed coaxially, and must for any one phyllosilicate be dependent upon the nature and behaviour of its immediate neighbours. I thus see no contradiction in finding triclinic phyllosilicate textures, measured on the scale of a few cubic millimetres, being associated with orthorhombic finite strain states, measured on the scale of hundreds of cubic centimetres, in slates.

PHILOSOPHICAL TRANSACTIONS OF THE ROYAL SOCIETY A MATHEMATICAL, PHYSICAL & ENGINEERING SCIENCES

Part of the work described in this study was done during the tenure of a Natural Environment Research Council Studentship, which is gratefully acknowledged. I also thank Professor J. G. Ramsay, Drs D. Dunnet, B. K. Tan and W. H. Owens for help and advice with the finite strain analyses; and M. T. Frost, P. Suddaby and K. O'Hara for help and advice with the texture analyses. I have benefitted from much stimulating discussion with Drs S. White and P. Williams, and with J. S. Whalley and R. J. Knipe, to whom I extend my thanks.

References (Siddans)

Baker, D. W., Wenk, H. R. & Christie, J. M. 1969 X-ray analysis of preferred orientation in fine-grained quartz aggregates. *J. Geol.* **77**, 144–172.

Bragg, R. H. & Packer, C. M. 1964 Quantitative determination of preferred orientation. *J. appl. Phys.* **35**, 1322–1328.

Clark, B. R. 1970 Mechanical formation of preferred orientation in clays. *Am. J. Sci.* **269**, 250–266.

Couterne, J. C. & Cizeron, G. 1971 Phénomène de défocalisation lié à la géométrie de la chambre de texture de Schulz et incidence sur l'intensité mesurée, *J. appl. Cryst.* **4**, 461–472.

Decker, B. F., Asp, E. T. & Harker, D. 1948 Preferred orientation determination using a Geiger-counter X-ray diffraction goniometer. *J. appl. Phys.* **19**, 388–392.

Dunnet, D. 1969 A technique of finite strain analysis using elliptical particles. *Tectonophysics* **7**, 117–136.

Dunnet, D. & Siddans, A. W. B. 1971 Non-random sedimentary fabrics and their modification by strain. *Tectonophysics* **12**, 307–325.

Elliott, D. 1970 Determination of finite strain and initial shape from deformed elliptical objects. *Geol. Soc. Am. Bull.* **81**, 2221–2236.

Etheridge, M. A. & Lee, M. F. 1975 Microstructure of slate from Lady Loretta, Queensland, Australia. *Geol. Soc. Am. Bull.* **86**, 13–22.

Feng, C. 1965 Determination of relative intensity in X-ray reflection study. *J. appl. Phys.* **36**, 3432–3437.

Frey, M. 1970 The step from diagenesis to metamorphism in pelitic rocks during Alpine orogenesis. *Sedimentology* **15**, 261–276.

Helm, D. G. & Siddans, A. W. B. 1971 Deformation of a slaty lapillar tuff in the English Lake District: Discussion. *Geol. Soc. Am. Bull.* **82**, 523–531.

Knipe, R. J. 1974 Micro-macro finite strain comparisons of the slaty cleavage lithologies from North Wales. M.Sc. thesis, University of London, 81 p.

March, A. 1932 Mathematische Theorie der Regelung nach der Korngestalt bei affiner Deformation. *Z. Krislallogr.* **81**, 285–297.

Means, W. D. & Paterson, M. S. 1966 Experiments on preferred orientations of platy minerals. *Contrib. Min. and Pet.* **13**, 108–133.

Moon, C. F. 1972 The microstructure of clay sediments. *Earth-Sci. Rev.* **8**, 303–321.

Oertel, G. 1970 Deformation of a slaty, lapillar tuff in the Lake District, England. *Geol. Soc. Am. Bull.* **78**, 1173–1187.

Oertel, G. 1974 Unfolding of an anticline by reversal of observed strains. *Geol. Soc. Am. Bull.* **85**, 445–450.

Oertel, G. & Phakey, P. P. 1972 The texture of a slate from Nantlle, Caernarvon, North Wales. *Texture* **1**, 1–8.

Parrish, W. 1962 X-ray measurements with counter tubes. In *Advances in X-ray diffractometry and X-ray spectrography* (ed. W. Parrish). Eindhoven: Centrex Publishing Co.

Ramsay, J. G. 1967 *Folding and fracturing of rocks*. New York: McGraw-Hill.

Roberts, B. & Siddans, A. W. B. 1971 Fabric studies in the Llwyd Mawr Ignimbrite, Caernarvonshire, North Wales. *Tectonophysics* **12**, 283–306.

Roe, R. J. 1965 Description of cristallite orientation in polycrystalline materials. III. General solution to pole figure inversion. *J. appl. Phys.* **36**, 2024–2031.

Schulz, L. G. 1949 A direct method of determining preferred orientation of a flat reflection sample using a Geiger-counter X-ray spectrometer. *J. appl. Phys.* **20**, 1030–1033.

Tan, B. K. 1973 Determination of strain ellipses from deformed ammonoids. *Tectonophysics* **16**, 89–101.

Tenckhoff, E. 1970 Defocusing for the Schulz technique of determining preferred orientation. *J. appl. Phys.* **41**, 3944–3948.

Whalley, J. S. 1973 Finite strain and texture variation associated with folds in a greywacke sequence at Rhosneigr, Anglesey. M.Sc. thesis, University of London, 98 p.

White, S. 1974 Application of HVEM to metamorphic and structural geology. Pp. 317–322 in *High voltage electron microscopy* (ed. P. R. Swann, C. J. Humphreys & M. J. Goringe). London: Academic Press.

PHILOSOPHICAL TRANSACTIONS OF THE ROYAL SOCIETY A MATHEMATICAL, PHYSICAL & ENGINEERING SCIENCES

Discussion

N. J. Soper (*Department of Geology, University of Sheffield, Mappin Street, Sheffield S1 3JD*). Dr N. J. Soper asked Dr Siddans whether the bimodal distribution of chlorite basal planes shown on the X-ray fabric diagram of a Welsh slate did in fact relate to the observed attitudes of cleavage and bedding in the sample. This was confirmed by Dr Siddans. Dr Soper then suggested that the phyllosilicate fabrics displayed by sedimentary rocks in slate belts could perhaps be interpreted in terms of the two major strain episodes which these rocks have suffered. One is uniaxial shortening normal to the bedding, a volume reduction due to water loss during compaction and diagenesis, and the other the subsequent tectonic 'cleavage strain'. The former would be irrotational and emphasize an initial bedding anistropy, and the fabric produced would be passively rotated during the second strain towards the cleavage plane but could not in the general case become coincident with it. The cleavage fabric must therefore have been induced by some mechanism other than passive rotation; petrographic evidence indicates that it is a growth fabric and as such is not interpretable by the March Strain model. The shape and orientation of such strain markers as accretionary lapilli relate (in addition to the initial shape factor) essentially to these two strains. If certain geologically reasonable assumptions are made regarding the orientation of the two strains in relation to observed bedding, cleavage and linear extension fabric on the cleavage, their values can be obtained by iterative incremental methods. For the Lake District 'bird's eye-tuffs', current research by Mr A. M. Bell has shown that the 'bedding strain' was around 1.5:1.5:1 and the 'cleavage strain' was quite close to plane strain.

A. W. B. Siddans. Dr Siddans agreed with Dr Soper that during compaction and diagenesis of a mudstone, volume reduction due to expulsion of pore water may lead to an approximately uniaxial shortening normal to bedding. This can be seen for example in tectonically undeformed purple Permian mudstones, containing green spots, on the Alpes Maritimes. Dr Siddans also agreed with Dr Soper that many of the phyllosilicates in slates are the product of recrystallization. This is seen most clearly when the crystallography and chemistry of illites from mudstones and slates are compared. Dr Siddans thus agreed with Dr Soper that phyllosilicate textures in slates cannot be interpreted in terms of the March model.

Dr Siddans agreed with Dr Soper that the shape fabrics of such strain markers as accretionary lapilli, in slates, must relate to both diagenetic compaction and tectonic deformation. Although not familiar with the precise procedures used by Mr Bell in his Lake District studies, Dr Siddans agreed that provided certain reasonable geological assumptions are made, the deformation ellipsoids associated with both diagenetic compaction and tectonic deformation may be estimated. However, two problematical aspects of such calculations should be noted: (*a*) There may be further volume reduction during tectonic deformation, due to loss of lattice water during mineralogic changes, if the deformation is associated with pro-grade metamorphism; for example the breakdown of kaolinite and mixed layer illite-montmorillorite (*b*). The relative orientations and magnitudes of successive tectonic strain increments usually remain unknown.

PHILOSOPHICAL TRANSACTIONS OF THE ROYAL SOCIETY A MATHEMATICAL, PHYSICAL & ENGINEERING SCIENCES